

Three-dimensional matter-wave vortices in optical lattices

Tristram J. Alexander, Elena A. Ostrovskaya, Andrey A. Sukhorukov, and Yuri S. Kivshar
*Nonlinear Physics Centre and ARC Centre of Excellence for Quantum-Atom Optics, Research School of Physical Sciences and
 Engineering, Australian National University, Canberra ACT 0200, Australia*

(Received 25 January 2005; published 10 October 2005)

We reveal that a repulsive Bose-Einstein condensate confined in a three-dimensional (3D) optical lattice supports vortex states which are spatially localized in all three dimensions and possess highly nontrivial particle flow. We demonstrate that the lattice stabilizes extended vortex lines that are normally unstable to transverse modulations, and show that stable vortices localized inside the 3D lattice may be easily generated via a nonadiabatic loading process.

DOI: [10.1103/PhysRevA.72.043603](https://doi.org/10.1103/PhysRevA.72.043603)

PACS number(s): 03.75.Lm

Quantized vortices are a fundamental phenomenon in many fields of physics, from superfluids to nonlinear optics [1]. Dilute gas Bose-Einstein condensates (BECs) are an ideal system to study these ubiquitous objects, and vortex research in BEC now ranges from vortex generation [2] and formation of vortex lattices [3] to complex dynamics in rotating condensates [4]. However, in BEC research, and in almost all studies of vortices reported in other fields [1], the vortex in three dimensions (3D) is considered as an extended object forming a line. In this work we consider fully spatially confined vortex structures that may exist in 3D periodic trapping potentials, and answer the fundamental question how does breaking all continuous translational symmetries affect vorticity?

The effect of symmetry on superfluid flow and vorticity is one of the outstanding problems in BEC physics, and an optical lattice is a powerful tool for investigating this problem due to its flexibility. Two different studies so far have considered the effects of lattices on vorticity. The first one examined a condensate in a two-dimensional lattice, confined in the third dimension by a harmonic trap. This essentially two-dimensional system was found to possess remarkable vortex states of a matter wave localized in the lattice by Bragg reflection [5]. The second work considered a vortex line in a 3D BEC cloud loaded into a one-dimensional lattice [6]. This first examination of changing the symmetry along the vortex line revealed that the vortex is still *unstable to transverse modulations*.

In this work, we consider the general case of vortices in a system with no continuous translational symmetries, such as a 3D optical lattice. We show that particle circulation in the lattice generally has no 2D lattice analog, yet stationary vortex states with such circulations still possess a straight-line vortex axis. Furthermore, we show that these vortex states are one of two types, either strongly localized “vortex atoms” or “vortex crystals” with an arbitrary degree of localization. We reveal that the vortex atoms have highly nontrivial forms including diamond, pyramid and triangle states and correspondingly complex particle flows, while the vortex crystals have more simple particle circulations. We demonstrate that the vortex crystals may lock a vortex line into the lattice, and are robust, thus providing an example of a *stable vortex line* in a nonrotating physical system. Finally we demonstrate the feasibility of generating these vortex states by

loading condensates containing vortex lines into a 3D optical lattice, opening the way for an experimental observation of these localized states.

We model the macroscopic dynamics of a Bose-Einstein condensate with repulsive atomic interactions in a 3D optical lattice by the normalized Gross-Pitaevskii (GP) equation

$$i\frac{\partial\Psi}{\partial t} + \Delta\Psi - V(\mathbf{r})\Psi - |\Psi|^2\Psi = 0, \quad (1)$$

where Ψ is the complex matter-wave wave function, $\mathbf{r} \equiv (x, y, z)$, and $\Delta \equiv \partial^2/\partial x^2 + \partial^2/\partial y^2 + \partial^2/\partial z^2$. The characteristic spatial scale is $a_L = d/\pi$, where $d = \lambda/2 \sin(\theta/2)$ is the lattice period, λ is the wavelength of the light producing the lattice, and θ the angle between the counterpropagating beams. For a cubic lattice potential we take

$$V(\mathbf{r}) = V_0(\sin^2 x + \sin^2 y + \sin^2 z), \quad (2)$$

with the depth V_0 scaled by the lattice recoil energy $E_L = \hbar^2/2ma_L^2$. The characteristic time scale is defined as ω_L^{-1} , where $\omega_L^{-1} = \hbar/E_L$. We neglect any additional trapping potential as we are interested in the effects of spatial localization due to nonlinearity and the optical lattice.

Nonlinear effects are weak at low densities, and the properties of the condensate can be described by the linear eigenmodes of the trapping potential. In a periodic potential, these are the Floquet-Bloch modes characterized by a bandgap spectrum due to the Bragg reflection of matter waves from the periodic potential [7]. For the 3D potential (2) the gaps where the wave propagation is suppressed *in all spatial directions* only occur above a threshold value $V_0 = V_{th} \approx 2.24$ (see Fig. 1).

Nonlinearity can counter wavepacket spreading and allows localization of matter waves inside the spectral gaps in the form of stationary states called gap solitons [8]. To find these nonlinear states, we look for solutions of Eq. (1) in the stationary form $\Psi(\mathbf{r}, t) = \psi(\mathbf{r})\exp(-i\mu t)$, where μ is the chemical potential, and solve the eigenvalue problem for $\psi(\mathbf{r})$ using a numerical functional minimization technique [9]. For all our results we use a spatial cube with periodic boundary conditions having sides 8 or 12 lattice sites long and a resolution of 128 points per side. Figure 2 shows the dependence of the norm of a 3D gap soliton $N = \int |\Psi|^2 d\mathbf{r}$, on

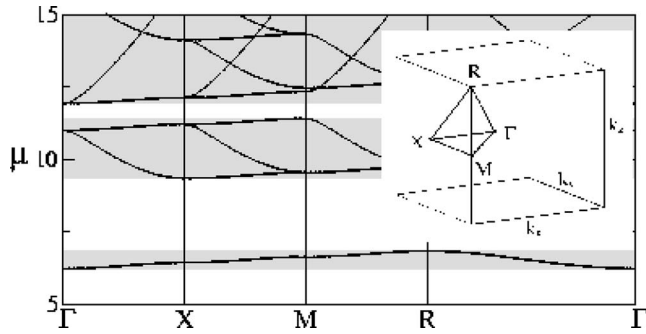


FIG. 1. Matter-wave bandgap spectrum $\mu(\mathbf{k})$ in a 3D optical lattice (2) at $V_0=6$. Shaded and open areas show bands and gaps, respectively. Inset shows the first Brillouin zone and the high-symmetry points in the reciprocal lattice.

the chemical potential within the first spectral gap, as well as examples of soliton density profiles. Despite a nontrivial phase of the wave function [see Fig. 2(c)], due to linear Bloch-wave tails, there is no particle flow in the soliton.

3D gap solitons have specific properties; near the lower gap edge they spread over many lattice sites being described by the free-space GP equation for an effective envelope of the corresponding Bloch state [10]. In this limit, the 3D gap solitons are unstable according to the Vakhitov-Kolokolov criterion since $\partial N/\partial\mu < 0$ [see Fig. 2(a)], and this instability may transform a broad state into a highly confined stable state deeper inside the gap [such as that shown in Figs. 2(b) and 2(c)]. The stability of these strongly localized states is confirmed by our numerical simulations of the soliton dynamics, which throughout are performed with a split-step propagation algorithm based on the fast Fourier transform.

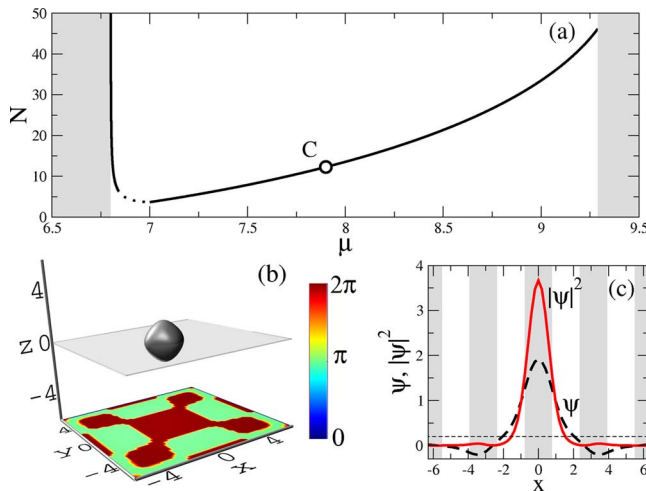


FIG. 2. (Color online) Family of 3D gap solitons ($V_0=6$). (a) Norm of the wave function N vs μ inside the gap; point C (at $\mu = 7.9$) corresponds to the state shown in (b) and (c). The curve near the lower band edge is calculated from the envelope approximation, with an interpolation between the two curves (dotted). (b) An isosurface of the soliton density, $|\psi|^2$, at the level $|\psi|^2=0.2$, with phase in the $z=0$ plane (semitransparent) shown below. (c) The cuts of ψ (dashed) and $|\psi|^2$ (solid) along the line $y=z=0$. Thin dashed line corresponds to $|\psi|^2=0.2$. Shaded areas show the lattice minima (parts of the potential less than $V_0/2$).

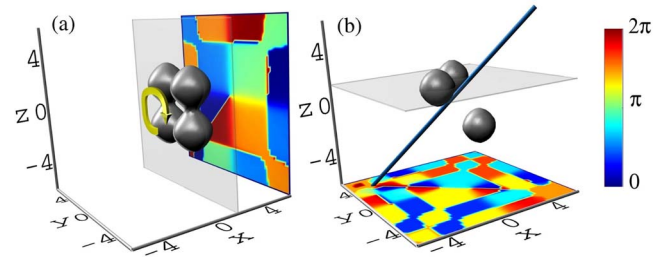


FIG. 3. (Color online) Examples of planar vortices for $V_0=6$ and $\mu=7.9$. (a) Off-site with axis corresponding to the X point and (b) equilateral triangle with axis given by the R point.

This method has inherent periodic boundary conditions which we supplement with absorbing potentials on the boundaries. In general, stability is determined with a 5% random perturbation of the initial state, over an evolution time $t=10^3$, which for ^{87}Rb in an optical lattice created with a $2\ \mu\text{m}$ period is approximately 1 s.

Next, let us consider the states with a circulating particle flow that are located in the gaps of the linear spectrum, the gap vortices. In order to find and study localized vortex states in the 3D lattice, we look for the structures composed of weakly interacting gap solitons in which there is no net particle exchange between the lobes. The field is then given by $\psi = \sum_m \psi_s(\mathbf{r}-\mathbf{r}_m) e^{i\phi_m}$ with the corresponding solvability condition [11],

$$\sum_{m=0}^{N-1} c_{nm} \sin(\phi_m - \phi_n) = 0, \quad (3)$$

where N is the number of solitons, ϕ_m is the phase of the m th soliton, and $c_{nm} \equiv c_{mn} = \iiint \psi_s(x-x_n, y-y_n, z-z_n) \psi_s^*(x-x_m, y-y_m, z-z_m) dx dy dz / \iiint |\psi_s(x, y, z)|^2 dx dy dz$ are the overlap integrals defining the coupling constants between solitons ψ_s located at the m th and n th sites. As Eqs. (3) are linear in c_{nm} , the coupling strengths can always be renormalized. The most important values are the sign of the coupling constants and the ratio of their strengths. We examine different geometries of the 3D vortex states with lobes given by the gap soliton shown in Figs. 2(b) and 2(c).

The simplest vortices in a 3D lattice are those in a plane. Such planar vortices have been predicted in 2D models of repulsive BEC [5]. Here we obtain planar vortices confined in the third dimension by Bragg reflection rather than a strong harmonic potential. We find direct analogs of the 2D gap vortices [5], including the off-site (centered on a lattice maximum) [see Fig. 3(a)] and on-site (centered on a lattice minimum) symmetry types, which as predicted by a solution of our equations (3), have a $\pi/2$ phase jump between lobes. Similar to the discrete models with attractive nonlinearity [12], we find that such planar states can be extremely robust, being stable over a wide range of their existence region.

Planar vortices also highlight one of the key differences between the 3D and 2D geometries. In the 2D lattice, the symmetric vortices must be either on-site or off-site. In the 3D lattice, these types persist but other symmetry axes become possible. The primary axes may be understood by ex-

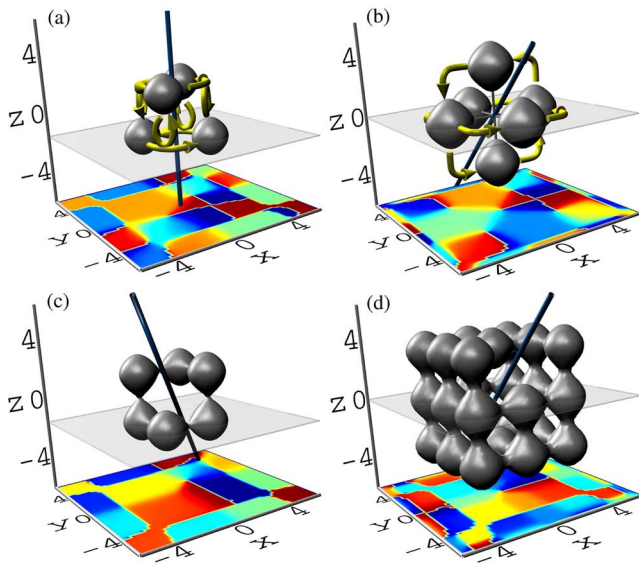


FIG. 4. (Color online) (a), (b) Vortex “atoms” and (c), (d) Vortex “crystals” at $V_0=6$, $\mu=7.9$. (a) Vortex pyramid with equal sides (X -point axis). (b) Vortex “diamond” (M -point axis). (c) Smallest vortex crystal with R -point axis and (d) broader vortex crystal with M -point axis symmetry. Arrows show complex particle flow and thick lines the vortex axes.

aming the Brillouin zone inset in Fig. 1. The axes of the 2D-like vortices correspond to the X point in the Brillouin zone, however, there are also the M -point (corresponding to an axis across the diagonal of a lattice square) and the R -point (the diagonal going through the center of the lattice cube) axes. Planar vortices in 3D may also have these M and R axes. One particularly interesting example is shown in Fig. 3(b), an equilateral triangle vortex. The triangle vortex is the most fundamental vortex state with discrete symmetry, possessing the minimum number of sites for circular particle flow. The remarkable fact is that in a 3D lattice this triangle state exists, even though the lattice has simple cubic symmetry. The possibility to embed symmetry states in a lattice of a different symmetry is one of the distinguishing features of optical lattices [11].

In general, vortices in a 3D lattice are not restricted to simple 2D planes; they are nonplanar with no 2D analog. We consider the most symmetric forms, which all possess a straight line vortex axis. We can expect from the earlier work on asymmetric vortices in 2D lattices [11] that an immense variety of vortex forms should exist in the full 3D system, but the existence of bent vortex lines in the lattice is still an open question. However, even within the high symmetry case we see a remarkable diversity of vortex states, which may be broadly classified into one of two groups, “vortex atoms” or “vortex crystals.” The vortex atoms we so name due to their distinct, but often unusual, symmetric configurations, such as the vortex pyramid [see Fig. 4(a)] and vortex diamond [see Fig. 4(b)]. A key characteristic of vortex atoms is their complex particle flow, as the examples in Figs. 4(a) and 4(b) show. Furthermore they are units of vorticity in the lattice and so can only be changed in discrete steps, equivalent to looking for bound states of two or more vortex atoms.

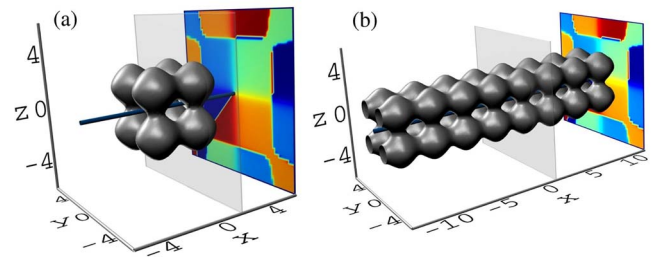


FIG. 5. (Color online) Examples of vortex crystals created by interacting planar vortices at $\mu=7.9$: (a) corotating coupled off-site vortices, (b) a “stack” of corotating vortices forming an extended vortex line.

The possibility of studying such vortex interactions is a powerful aspect of 3D lattices, however, an examination of the composite vortex states is beyond the scope of this work, and will be presented elsewhere.

The nature of the vortex crystals is quite different. Firstly, their form is not distinct, as their width can be arbitrarily increased to form wider states. Secondly, their particle flow simply circulates about the axis, unlike the complex flows seen in the vortex atoms. These states are in some sense the 3D generalization of the broad vortex states discussed earlier in 2D [5]. We show two examples: Fig. 4(c) is the simplest vortex crystal with an R -axis symmetry while Fig. 4(d) is an example of a broader vortex crystal with an M axis. Even the planar vortices may be classified according to the definitions of the vortex atoms and crystals: Fig. 3(a) shows the smallest vortex crystal and Fig. 3(b) the smallest vortex atom.

One of the important problems of the physics of vortices is the instability of a vortex line due to transverse modulations [13]; vortex-line bending is one of the feature experiments in BEC physics [14]. In a 3D lattice this transverse instability can be suppressed. All of the vortex crystals contain straight vortex lines, of either X -, M -, or R -axis type, and in general these lines are very robust. As an example of the construction of a vortex crystal and a depiction of the most localized extended vortex line, we consider the planar vortex of Fig. 3(a) as a basis. Instead of extending the vortex crystal transversely we consider a longitudinal build-up around the vortex axis. This leads to a stack of anything from two [see Fig. 5(a)] to many planar vortices [see Fig. 5(b)].

We have found that these extreme aspect ratio vortices are very robust, showing no instability at $t=10^3$, with the line trapped by the lattice. Of course, we may extend these vortices transversely to obtain broader, higher particle number states.

Finally, we discuss the key question of how localized matter-wave vortices might be generated in a 3D lattice. A full analysis of this question will be presented elsewhere, however, here we simply state one of our most important results: generation of a specific nonlinear state is best done nonadiabatically. With this in mind, we first consider a cigar-shaped condensate with a vortex line, initially confined in a harmonic trap and then instantaneously released into a 3D optical lattice, as shown in Figs. 6(a) and 6(b). In this case, for a cigar-shaped trap with the aspect ratio of 20 and the maximum of the initial transverse wave function approxi-

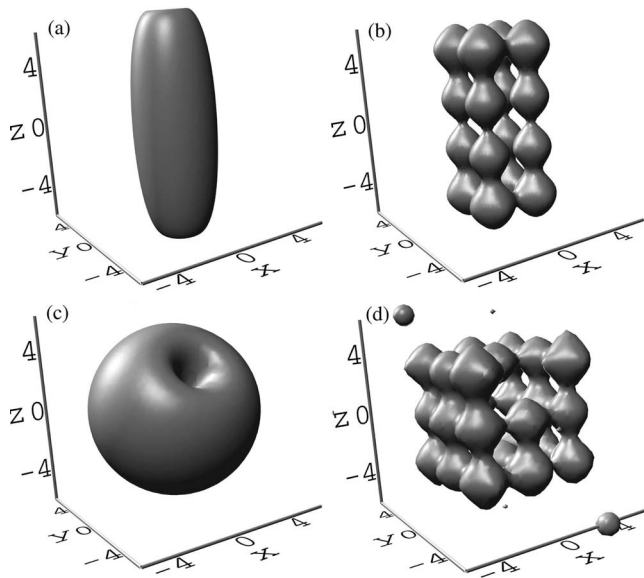


FIG. 6. Generation of localized vortices in the 3D lattice from a harmonic trap. (a) Cigar-shaped vortex initial condition ($t=0$). (b) Vortex stack generated dynamically ($t=41$). (c) Vortex in spherical condensate with axis inclined relative to the lattice ($t=0$) (5000 atoms for a $2 \mu\text{m}$ period). Output state at $t=50$ showing dynamical generation of a vortex crystal (3000 atoms. Approximate maximum densities: initial $1 \times 10^{-14} \text{ cm}^{-3}$; final $8 \times 10^{-13} \text{ cm}^{-3}$).

mately located on the minimum of the potential, the condensate forms the nonlinear vortex-stack state centered on a lattice maximum [see Fig. 5(b)] inside the linear gap. The

length of the stack depends on the length of the initial cigar, and it is highly robust against transverse modulations of the vortex line. If instead we start with the more general case of a vortex in a spherical condensate, we find that this initial state will form a broad localized vortex crystal state. To show the generality of this process, we consider an initial vortex state with an axis aligned with the M axis of the lattice. Despite the difference between the initial condition and the nonlinear state in the lattice we see a clear formation of the vortex crystal, in this case the M axis state shown in Fig. 4(d). The only requirement is that the maximum of the initial density is in or above the first band gap. Initial excitations are damped as particles are lost from the condensate, and the vortex drops into the linear band gap where it is localized. Generation of the smaller vortex atoms and their bound states is a more delicate affair and will be discussed elsewhere.

In conclusion, we have predicted the existence of novel classes of spatially localized vortex structures in Bose-Einstein condensates loaded into three-dimensional optical lattices. In particular we have identified a broad class of vortices which are remarkably robust, and demonstrated that they may be generated in experiment through a simple non-adiabatic loading of the lattice. Furthermore, we have revealed that these vortices have a simple phase structure, and are therefore amenable to phase interferometry techniques for detection.

We acknowledge Markus Oberthaler and Randy Hulet for useful discussions of the experimental realizations. This work was supported by the Australian Research Council.

-
- [1] L. M. Pismen, *Vortices in Nonlinear Fields* (Clarendon Press, Oxford, 1999).
- [2] M. R. Matthews, B. P. Anderson, P. C. Haljan, D. S. Hall, C. E. Wieman, and E. A. Cornell, *Phys. Rev. Lett.* **83**, 2498 (1999); K. W. Madison, F. Chevy, W. Wohlleben and J. Dalibard, *ibid.* **84**, 806 (2000).
- [3] J. R. Abo-Shaeer, C. Raman, J. M. Vogels and W. Ketterle, *Science* **292**, 476 (2001).
- [4] V. Bretin, S. Stock, Y. Seurin, and J. Dalibard, *Phys. Rev. Lett.* **92**, 050403 (2004).
- [5] E. A. Ostrovskaya and Yu. S. Kivshar, *Phys. Rev. Lett.* **93**, 160405 (2004).
- [6] J. P. Martikainen and H. T. C. Stoof, *Phys. Rev. Lett.* **93**, 070402 (2004).
- [7] F. Bloch, *Z. Phys.* **52**, 555 (1928).
- [8] O. Zobay, S. Potting, P. Meystre and E. M. Wright, *Phys. Rev. A* **59**, 643 (1999); P. J.Y. Louis, E. A. Ostrovskaya, C. M. Savage, and Yu. S. Kivshar, *ibid.* **67**, 013602 (2003); B. Eiermann, Th. Anker, M. Albiez, M. Taglieber, P. Treutlein, K. -P. Marzlin and M. K. Oberthaler, *Phys. Rev. Lett.* **92**, 230401 (2004); V. Ahufinger, A. Sanpera, P. Pedri, L. Santos, and M. Lewenstein, *Phys. Rev. A* **69**, 053604 (2004).
- [9] J. J. Garcia-Ripoll and V. M. Perez-Garcia, *SIAM J. Sci. Comput. (USA)* **23**, 1316 (2001).
- [10] H. Pu, L. O. Baksmaty, W. Zhang, N. P. Bigelow, and P. Meystre, *Phys. Rev. A* **67**, 043605 (2003).
- [11] T. J. Alexander, A. A. Sukhorukov, and Yu. S. Kivshar, *Phys. Rev. Lett.* **93**, 063901 (2004).
- [12] P. G. Kevrekidis, B. A. Malomed, D. J. Frantzeskakis, and R. Carretero-Gonzales, *Phys. Rev. Lett.* **93**, 080403 (2004).
- [13] L. P. Pitaevskii, *Sov. Phys. JETP* **13**, 451 (1961).
- [14] P. Rosenbusch, V. Bretin and J. Dalibard, *Phys. Rev. Lett.* **89**, 200403 (2002).